Progress In Electromagnetics Research, Vol. 138, 519–536, 2013

COMPARISON OF THE TWO-SCALE AND THREE-SCALE MODELS FOR BISTATIC ELECTROMAGNETIC SCATTERING FROM OCEAN SURFACES

Hejia Luo and Yang Du*

The Department of Information Science and Electronics Engineering, Zhejiang University, Hangzhou 310027, China

Abstract—With rapid development of satellite technology in monitoring the ocean, a good understanding of the physical processes involved in the electromagnetic ocean-surface interaction is required. The composite surface models are usually applied in the analysis of the interaction, hence a systematical check of their region of validity is desirable. Based on a generalized minimal residual procedure which is right preconditioned (GMRES-RP) that we have recently developed which has demonstrated the desirable properties of a numerical algorithm: robust and efficient, in this paper, for bistatic scattering from one dimensional ocean surfaces, we carry out a systematic assessment of the performance of the popular two-scale model and the advanced three-scale model under different conditions of ocean surface wind speeds, polarizations, frequencies, and incidence angles. It is found that the two-scale model in general captures the bistatic scattering pattern, yet the accuracy of geometrical optics (GO) for the large scale wave brings considerable impact on the overall accuracy. If the evaluation of the contribution of the large scale wave is instead using direct numerical integration for the corresponding Kirchhoff integral, impressive improvements are frequently observed, especially at low frequency (L and C bands) and low wind speed (3 m/s). But care should be taken when apply two-scale method with numerical integration, since there are cases where visible discrepancy with method of moment (MoM) are observed. On the other hand, the three-scale model is found in very good agreement with MoM across the considered ocean surface wind speeds, polarizations, frequencies, and incidence angles, hence represents a much advanced model over the two-scale model.

Received 21 February 2013, Accepted 15 March 2013, Scheduled 3 April 2013

* Corresponding author: Yang Du (zjuydu03@zju.edu.cn).

1. INTRODUCTION

The ocean is a fundamental part of the climate system, and the monitoring of its state is of primary importance. The use of microwave remote sensing for such task has been growing, such as the SMOS [1] and WindSAT [2] missions. In exploiting the available information, physically based inverse procedures call for high fidelity scattering/emission models.

The two-scale model (TSM) has been one of the most widely used models for ocean surface scattering [3–6]. In this model an ocean surface is treated as a composite surface which contains two scales of waves: the large and small scales, with the latter being tilted, advected and modulated by the former. Scattering from the large scale wave is assumed by the quasi-specular theories, whereas that from the small scale by Bragg scattering. The effects of the large scale wave on the small one have generally been through an averaging procedure with respect to the probability distribution of the slope of the long wave.

A notable advance over the TSM on the ground of composite surface assumption is the so called three-scale model (T3SM) [7, 8], where the ocean surface is successively split into regions from which the scatter comes from small-, intermediate-, and large-scale waves. The appeal of this model is that it allows a gradual transition from Bragg scattering to Kirchhoff scattering in a manner dependent on incidence angle, wind speed, and ocean spectrum. In this model, the assumption about classic Bragg scattering for small scale waves and classic quasi-specular scattering for large-scale waves is still retained. Direct contribution from the intermediate-scale waves is through the evaluation of the Kirchhoff integral. The incidence angles for the small- and intermediate waves are corrected accordingly. Scattering from the large- and intermediate waves are attenuated by the smaller scale waves. This attenuation leads to a feature essentially different from that of TSM: the large scale wave dominates the scattering at small incidence angles in the TSM, whereas it is rarely important in the T3SM.

The conceptually simple and convenient to use TSM are still widely used today, either in its conventional form [9, 10] or modified versions [11, 12]. In [10], comparison is made of emissivity evaluated from three models: the TSM, the small slope approximation/small perturbation method (SSA/SPM) model [9, 13], and an empirical model. It is found that for low and medium wind conditions, these three models roughly agree on a linear increase yet with different slopes of emissivity with wind speed; nevertheless, the discrepancy becomes appreciable under intense wind conditions.

It is thus desirable to carry out a systematic assessment of the performance of the TSM and its less well known sibling the T3SM. Ideally this investigation would be conducted for two-dimensional (2-D) ocean surface scattering against exact numerical results. However, albeit the readily available formalisms of these analytical models for 2-D surfaces, a numerical approach that is capable of including the effects of surface waves of all scale, in particular of the large scale, is still elusive at present. We have to compromise and resort to the one-dimensional (1-D) surface instead. However, even in this seeming simple setting things can become challenging if 1) wind speed becomes considerably large; 2) incidence angle approaches near grazing. In addition, since the numerical results are expected to serve as the benchmark, considerably large number of realizations, say, 500 or 1000, needs to be performed to provide adequately accurate results; as such, the adopted numerical approach is required to be of high efficiency and robustness.

To the last requirement we are in a good position. Recently we have developed a highly efficient and robust numerical method for the analysis of scattering from randomly rough surfaces. In this method, a generalized minimal residual procedure which is right preconditioned (GMRES-RP) [14] with the forward-backward method (FBM) [15], in combination with the spectral acceleration (SA) [16, 17] technique to expedite the computation of matrix-vector product. The applied preconditioning is found to transform the original linear system from near singular to stable with a good condition number; specifically, the spectrum of the preconditioned matrix is found condensed in the vicinity of the point 1 in the complex plane, an indicator of the good approximation quality of the preconditioner to the original matrix. Moreover, the fact that the construction of the preconditioner does not require the knowledge of the distribution of the impedance matrix spectrum implies that the proposed method can be used as a general purpose iterative solver. The proposed method has demonstrated the desirable properties of a numerical algorithm: robust and efficient. Although this method was originally designed for single scale surface (Gaussian spectrum), there is no difficulty in extending it to the composite ocean surface.

In this study, with the GMRES-RP serves as benchmark, we intend to assess the predictive power of TSM and T3SM of bistatic scattering from ocean surfaces, in a systematical manner under different conditions of ocean surface wind speed, polarization, frequency, and incidence angle. Here we focus on the bistatic scattering rather than the conventionally considered backscatter, since the evaluation of emissivity calls for bistatic scattering coefficient [18],

as well as the growing trend of bistatic applications [19–21]. The findings, although by nature are for 2-D scattering from 1-D ocean surface due to computer limitations, can nevertheless be expected to provide valuable insight into the full 3-D surface scattering problem.

2. THE TWO-SCALE MODEL AND THREE-SCALE MODEL

2.1. The Two-scale Model

The TSM model divides the surface into large and small scale waves. Scattering from the large scale wave is evaluated with the Kirchhoff approximation (KA), which is given by [22]

$$\sigma^{ol}(\theta_i,\theta_s) = k\left|\frac{1+\cos(\theta_s+\theta_i)}{\cos\theta_i+\cos\theta_s}\right|^2 \int_{-\infty}^{\infty}\frac{dr}{2\pi}\exp(ik_{dx}r) \left[\exp\left(k_{dz}^2h_l^2(\rho_l(r)-1)\right)-\exp\left(-k_{dz}^2h_l^2\right)\right] \quad (1)$$

where k is the microwave wavenumber, h_l the rms height of the large scale wave, and $h_l^2\rho_l$ the correlation function, θ_i and θ_s are the incidence angle and scattering angle, respectively, and

$$k_{dz} = -(k_{iz}+k_z) = -(k\cos\theta_i + k\cos\theta_s), \quad (2)$$

$$k_{dx} = k_{ix}-k_x = k\sin\theta_i - k\sin\theta_s. \quad (3)$$

It should be noted that the definition of scattering coefficient here is different from that in [22] by a factor $\cos\theta_i$ so that the integration of σ^{ol} over all scattering angles is $\cos\theta_i$ rather than unity. The bistatic scattering coefficient of (1) is commonly evaluated through the geometric optics (GO) approximation to yield

$$\sigma^{ol}(\theta_i,\theta_s)=\frac{1}{\sqrt{2\pi}v_s}\frac{|1+\cos(\theta_s+\theta_i)|^2}{|\cos\theta_i+\cos\theta_s|^3}\exp\left(-\frac{(\sin\theta_i-\sin\theta_s)^2}{2(\cos\theta_i+\cos\theta_s)^2v_s^2}\right). \quad (4)$$

where v_s is the rms slope.

The contribution from the small scale wave is due to Bragg scattering, which is evaluated using the small perturbation method (SPM). The expression for the first order SPM solution is

$$\sigma_{pp}^{os_l}(\theta_i',\theta_s') = \frac{4(k_zk_{iz})^2|B_{pp}|^2}{k}W(k_{dx}) \quad (5)$$

where $B_{hh} = -1$ for HH polarization and $B_{vv} = \frac{(1-\sin\theta_i\sin\theta_s)}{\cos\theta_i\cos\theta_s}$ for VV polarization. $W(k) = \frac{S(k)}{2}$ for 1-D surface, and $S(k)$ is the ocean spectrum (The case of Elfouhaily spectrum is given in the Appendix).

The primed θ_i' and θ_s' denote the local angles (incidence and scattered) due to the tilting of the large-scale waves, whose effect should be fully accounted for by the averaging over the probability distribution $P(s)$ of the slope s.

$$\sigma_{pp}^{os}(\theta_i, \theta_s) = \int_{-\infty}^{\infty} ds\ \sigma_{pp}^{osl}\left(\theta_i', \theta_s'\right) P(s) \tag{6}$$

2.2. The Three-scale Model

Reasoning that the Kirchhoff integral was derived under the assumptions about homogeneous and stationary surface waves, which are not valid for the sea surface on small time and space scales, Plant [7] proposed to partition the sea surface into large, intermediate, and small scale waves, and treated the larger scales deterministically in averages over smaller scales. These filtered surfaces, large, intermediate, and small, are assumed that each exhibits Gaussian statistics. Statistical independence and phase decorrelation are further assumed among different scales to allow the decomposition of the surface correlation function into the three-scale components as

$$h^2\rho = h_l^2\rho_l + h_i^2\rho_i + h_s^2\rho_s \tag{7}$$

where the correlation coefficients ρ_α, $\alpha = l,\ i,\ s$, when a specific scale is under consideration, are taken to be unity over the larger scale and null over the smaller scale. Correspondingly, the Kirchhoff integral, which is the starting point and takes the following form:

$$\begin{aligned}\sigma_{pp}^{o}(\theta_i, \theta_s) = & \frac{4(k_z k_{iz})^2 |B_{pp}|^2}{k k_{dz}^2} \int \frac{dr}{2\pi} \exp(ik_{dx} r) \\ & \left[\exp\left(k_{dz}^2 h^2 (\rho(r) - 1)\right) - \exp\left(-k_{dz}^2 h^2\right)\right]\end{aligned} \tag{8}$$

is treated separately for the three-scales as follows:

1) The small scale wave (SSW), which contributes to the scattering coefficient by Bragg scattering, is evaluated using SPM as given by (5) and (6).

2) Direct contribution of the intermediate scale wave (ISW) is

$$\begin{aligned}\sigma_{pp}^{oi_l}\left(\theta_i', \theta_s'\right) = & \frac{4(k_z k_{iz})^2 |B_{pp}|^2}{k k_{dz}^2} \exp\left(-k_{dz}^2 h_s^2\right) \\ & \int_{-i}^{+i} \frac{dr}{2\pi} \exp(ik_{dx} r) \left[\exp\left(k_{dz}^2 h_i^2 (\rho_i(r) - 1)\right)\right]\end{aligned} \tag{9}$$

where the primed angles are due to the tilting of the large scale waves, so a similar averaging process needs to be performed to fully account for the probability distribution of the slope of the large scale wave.

3) The direct contribution of the large scale wave (LSW) is

$$\sigma_{pp}^{ol}(\theta_i,\theta_s) = \frac{4(k_z k_{iz})^2 |B_{pp}|^2}{k k_{dz}^2} \exp\left(-k_{dz}^2\left(h_s^2+h_i^2\right)\right) \int_{-\infty}^{+\infty} \frac{dr}{2\pi} \exp\left(ik_{dx}r\right)\left[\exp\left(k_{dz}^2 h_l^2\left(\rho_l(r)-1\right)\right)\right] \quad (10)$$

which is commonly approximated by the GO method. Yet unlike in the conventional 2SM, here the large scale wave is attenuated by a factor $\exp(-k_{dz}^2(h_s^2+h_i^2))$ as evident in (10), attributing to the intermediate and small waves. The effect of the attenuation is that the contribution of the large-scale wave is rarely important, in contrast to the 2SM theory that below the incidence angles of about 10° to 20°, backscatter from the large scale waves dominates. The contribution from intermediate scale waves (ISW) in most cases takes the dominant role with respect to the LSW, and is affected by both the large scale and small scale waves: the former tilts the local incidence and scattering angles, and the latter provides an attenuating factor $\exp(-k_{dz}^2 h_s^2)$.

3. PERFORMANCE COMPARISONS

In this section, we assess the performances of TSM and T3SM for bistatic scattering from ocean surfaces under different conditions of ocean surface wind speed, polarization, frequency and incidence angle. The benchmark is the MoM numerical results, which are provided by the GMRES-RP method. The ocean surface is assumed to be perfectly conducting in this study for the frequencies considered in the microwave region, which is a reasonable assumption in active remote sensing [23]. More importantly, there is also consideration regarding the fidelity/complexity balance of alternative approaches. For instance, if the ocean is modeled as a thick dielectric slab, then at sea surface temperature (SST) of 15°C, sea surface salinity (SSS) of 25‰, at 10 GHz (X band), the relative dielectric constant of sea is $54.3 + i38.6$. Hence at a wind speed of 10 m/s, to include the effect of all surface wave scales, assuming a cutoff wavenumber of $k_{dl} = 0.03$, a quick check reveals that around 7 thousand wavelengths are required, which translates to over 8 hundred thousand surface unknowns. With larger wind speed and higher frequencies, the task can readily become impractical. Yet if the impedance boundary condition (IBC) is used instead, although the finite conducting property of ocean can be partly captured, IBC itself is an approximate method, which makes it difficult to single out, at the presence of different performances of TSM and T3SM, which part is attributed to the inherent difference between these

two models, and which part to the inadequate approximation of IBC. The surface length is $L = 16384\lambda$ unless specified otherwise. With a sampling rate of 8 points per wavelength, this gives a total number of surface unknowns of 131072. The error tolerance for iteration is set to be 10^{-4}. Monte Carlo simulations are averaged over 500 realizations to obtain stable results.

In the study the cutoff wavenumber for TSM is set as $k/2\cos(\theta_i)$ where k is the microwave wavenumber and θ_i is the incidence angle [24]. The cutoff wavenumbers for T3SM are k_2 by which $4k^2\cos^2\theta_i \int_{k_2}^{\infty} S(k)dk = 0.09$ for SSW and ISW separation and k_1 by which $4k^2\cos^2\theta_i \int_{k_1}^{k_2} S(k)dk = 9$ for ISW and LSW separation [7]. The Elfouhaily spectrum is employed [25]. It was derived from oceanographic and wave tank measurements, with the nice property that the surface slope distribution derived by this spectrum is in agreement with the Cox-Munk distribution [25]. To describe ocean surfaces, besides the Elfouhaily spectrum, there are other popular spectra, including the Pierson-Moskowitz (PM) spectrum [26] and the Durden-Vesecky (DV) spectrum [27]. The differences among the three spectra lie primarily in the short wave portion of the spectrum, where PM spectrum dose not include surface tension effect and simplifies the Leykin-Rosenberg region by using a straight line on a log-log plot of the spectrum versus wave number [28].

We begin by examining the accuracy of GMRES-RP for ocean surface scattering, where its normalized bistatic scattering coefficients (NBSCs) are compared with that of direct matrix inversion (DMI). We intentionally make the ocean surface as rough and the surface unknowns as large as possible, so the time and memory complexity issues as well as the effectiveness of handling the singularity of the impendence matrix Z are checked out. The wind speed U (19.5) is set 15 m/s, which is the upper bound in the current study since the wind speed of 15 m/s is generally held to be the limit where the ocean can be approximated by a linear spectrum. The surface length L is 8192λ, so the number of surface unknowns is 65536 with a sampling rate of eight points per wavelength, a number of unknowns close to the limit of performing DMI in our server. The corresponding k_{dl} is $2\pi/L$, and the *rms* heights are 1.24 m at 5.3 GHz and 0.91 m at 19 GHz, respectively, which translate to $kh = 137.7$ and 363.4 at these two frequencies, a number quite large. For these large number of unknowns, the DMI is very slow and we compare its results with the GMRES-RP solution at 5.3 GHz and 19 GHz. The incident angle is 60°. Across the scattered angles from −90° to 90°, the agreement is within 0.15% for all the cases that we have tested.

We start the comparison at low frequency (L band) and small wind

speed (3 m/s). For TSM at $\theta_i = 20°$ (which is the incidence angle we will use for the next several numerical experiments, and later when we change the incidence angle we shall mention explicitly), the *rms* height of the LW wave is $h = 0.0494$ m, thus $kh\cos\theta_i = 1.360$. This value is below the established criterion for GO where $kh(\cos\theta_i + \cos\theta_s)$ is required at least to be 3.16 [29]. As such, the GO contribution to TSM is expected not to be adequately accurate. This is indeed the case, as shown in Fig. 1 for both HH and VV polarizations. It is observed that the TSM model, although captures the general pattern, shows appreciable discrepancies at the scattering angle sets around $-20°$ (backscattering) and 60°, for the latter the discrepancy can be up to around 4 dB.

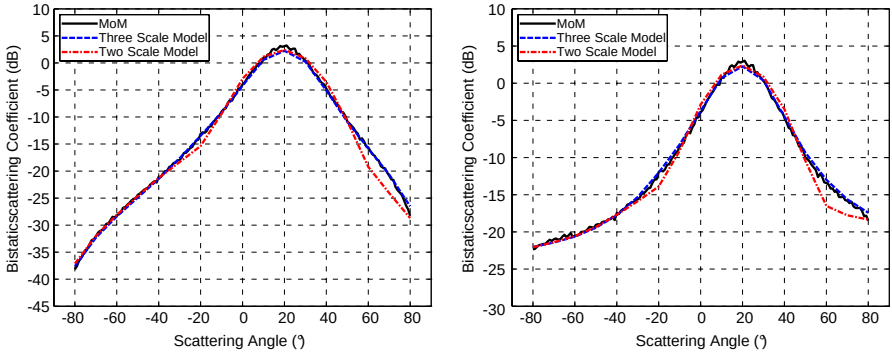

(a) Horizontal polarization (b) Vertical polarization

Figure 1. Bistatic scattering comparison of numerical method, TSM, and T3SM. L band. Incidence angle: 20°. Wind speed: 3 m/s. (a) HH, and (b) VV.

On the other hand, in the T3SM, the inadequate accuracy of GO in the evaluation of LSW contribution is suppressed since the direct contribution from LSW is rarely important. The integral associated with the intermediate scale waves is evaluated numerically as in [7] hence is sufficiently accurate. The results are also plotted in Fig. 1 for comparison. It shows that T3SM agrees very well with MoM across the scattered angles.

When the wind speed increases to 10 m/s, for TSM, $h = 0.56$ m and $kh\cos\theta_i = 15.46$, which means LSW enters the GO region across the scattering angle range $[-90°, 90°]$. The results (shown in Fig. 2) improves over Fig. 1 substantially, in particular in the backscattering direction, yet the discrepancy with MoM is still visible at θ_s around 80°. In contrast, the T3SM model again is in perfect agreement with MoM.

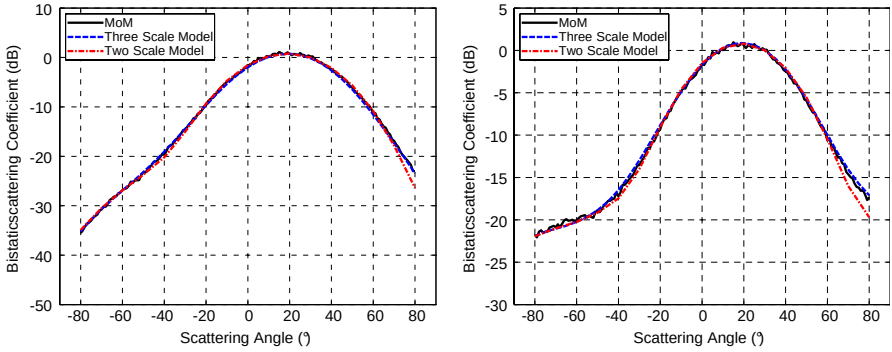

(a) Horizontal polarization (b) Vertical polarization

Figure 2. Bistatic scattering comparison of numerical method, TSM, and T3SM. L band. Incidence angle: 20°. Wind speed: 10 m/s. (a) HH, and (b) VV.

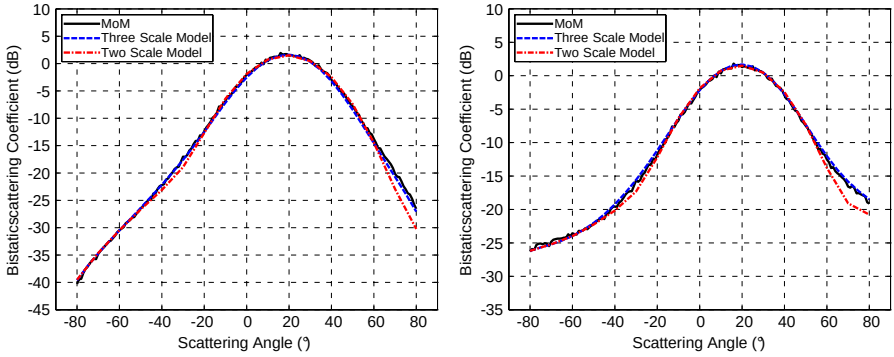

(a) Horizontal polarization (b) Vertical polarization

Figure 3. Bistatic scattering comparison of numerical method, TSM, and T3SM. C band. Incidence angle: 20°. Wind speed: 3 m/s. (a) HH, and (b) VV.

If we further increase the wind speed to 15 m/s, the results for TSM get slightly better, yet the discrepancy at θ_s around 80° is still present.

At C band and a wind speed of 3 m/s, for LSW of TSM, $h = 0.0495$ m and $kh\cos\theta_i = 5.16$, suggesting that GO approximation can be used for LSW. The results are shown in Fig. 3. We observe better agreement than the L band counterpart is obtained, in particular in the backscattering direction. Nevertheless appreciable discrepancy (up

to 3.5 dB) is present in the forward direction. The T3SM is again in excellent agreement with MoM.

At higher frequency and large wind speed, the agreement between TSM and MoM becomes even better, as illustrated in Fig. 4 for the case of Ka band and large wind speed (15 m/s). The T3SM is seen in perfect agreement with MoM.

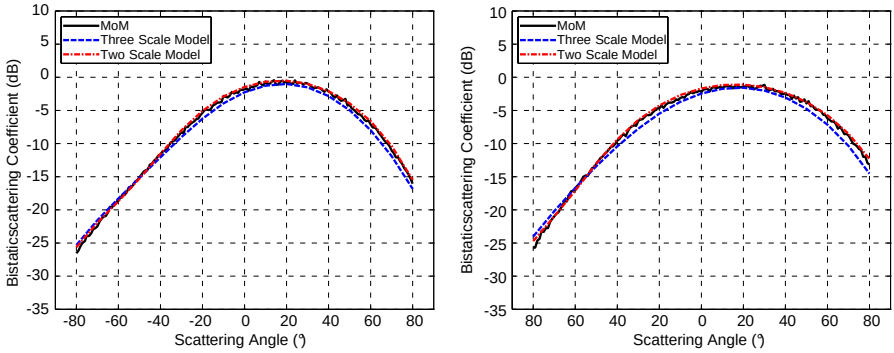

(a) Horizontal polarization (b) Vertical polarization

Figure 4. Bistatic scattering comparison of numerical method, TSM, and T3SM. Ka band. Incidence angle: 20°. Wind speed: 15 m/s. (a) HH, and (b) VV.

To gain deeper understanding of their scattering behaviors, we decompose the scattering components of the TSM and T3SM. The case of Fig. 3 is shown in Fig. 5 for HH polarization. We first examine the TSM model (Fig. 5(a)). The GO contribution is expected to dominate in the specularly forward direction, as indicated by the multiplicative factor $\exp(-\frac{(\sin\theta_i-\sin\theta_s)^2}{2(\cos\theta_i+\cos\theta_s)^2 v_s^2})/v_s$ in the GO expression for small *rms* slope v_s. In the backward direction, after the sharp fall-off of GO starting at around $-20°$, the SSW takes the dominant role from $-30°$ afterwards and provides an almost perfect result for scattering angle beyond $-45°$.

In the T3SM, the SSW behavior is similar to that of TSM. The direct contribution of LSW can be completely ignored when compared to that of ISW and SSW, which manifests the effect of the discounting factor $e^{-k_{dz}^2(h_i^2+h_s^2)}$. In the forward direction, the ISW dominates, which falls off at around $\theta_s = 60°$, yet in a much moderate manner (it is 10 dB higher than the LSW in TSM at $\theta_s = 80°$). Along with the slightly higher SSW, T3SM is in almost perfect agreement with the MoM.

In view of the above observations, we are prompted with the

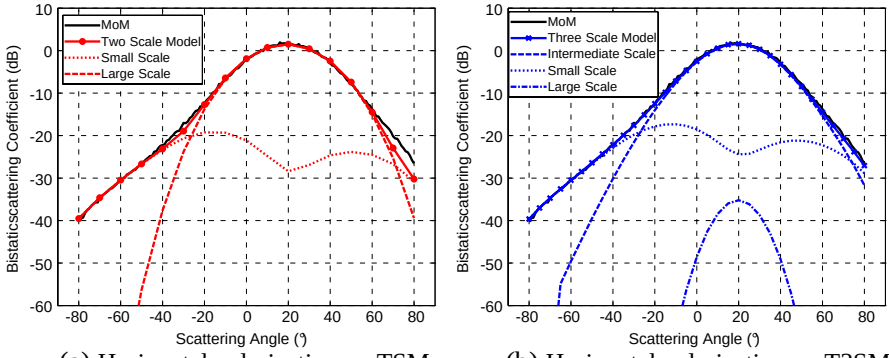

(a) Horizontal polarization --- TSM (b) Horizontal polarization --- T3SM

Figure 5. Component waves contribution to bistatic scattering. C band. Incidence angle: 20°. Wind speed: 3 m/s. HH polarization. (a) TSM, and (b) T3SM.

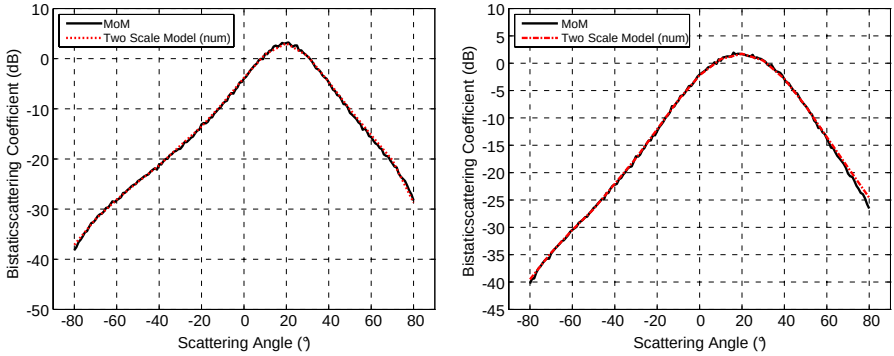

(a) L band, Horizontal polarization (b) C band, Horizontal polarization

Figure 6. Bistatic scattering comparison of TSM with numerical integration for LSW with MoM. HH polarization. Incidence angle: 20°. Wind speed: 3 m/s. (a) L band, and (b) C band.

conjecture that the first order SPM is adequately accurate, and that the discrepancy of TSM with MoM mainly stems from the inadequate accuracy of GO. For this purpose we evaluate the Kirchhoff integral for LSW, that is, the integral appearing in (1), numerically rather than using GO approximation in the TSM. The results are shown in Fig. 6 for HH polarization at C and L bands, corresponding to Fig. 1(a) and Fig. 3(a). The almost perfect agreements verify the conjecture.

Further comparisons at higher bands are shown in Fig. 7 for Ku band and Fig. 8 for Ka band at the small wind (3 m/s) and HH

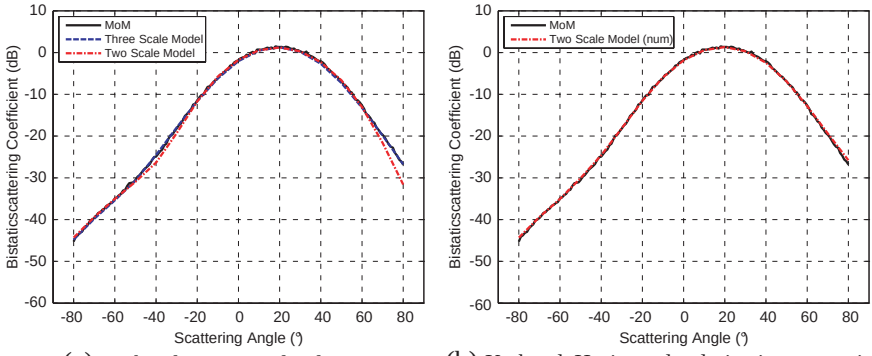

(a) Ku band, Horizontal polarization (b) Ku band, Horizontal polarization, numerical

Figure 7. Bistatic scattering comparison. Ku band. Incidence angle: 20°. Wind speed: 3 m/s. HH polarization. (a) TSM and T3SM. (b) TSM with numerical integration for LSW.

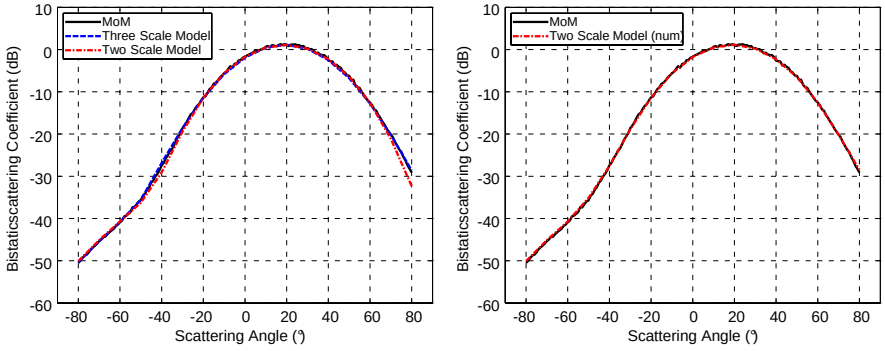

(a) Ka band, Horizontal polarization (b) Ka band, Horizontal polarization, numerical

Figure 8. Bistatic scattering comparison. Ka band. Incidence angle: 20°. Wind speed: 3 m/s. HH polarization. (a) TSM and T3SM. (b) TSM with numerical integration for LSW.

polarization. It is seen that the T3SM is always in perfect agreement with MoM, while the TSM can be in perfect agreement as well if the LSW contribution is numerically evaluated. The same observations apply to VV polarization as well.

For moderate or high wind speed (10 m/s or 15 m/s, respectively), the same observations apply, although the improvement of TSM via the numerical integration over the GO for LSW is not as large since it is found that TSM (with GO) tends to perform better at higher wind speed.

It is appropriate here to stress the point that TSM via the numerical integration, although shows impressive improvement over its analytical counterpart TSM (with GO), is not yet the panacea for the analysis of ocean scattering even in the case of 1-D surfaces. For instance, at L band, small wind (3 m/s), and 40° incidence angle, Fig. 9 shows that the numerical TSM is in visible discrepancy with MoM at $\theta_s = 80°$. This discrepancy cannot be simply suppressed by the inclusion of shadowing effect, since its VV result is already underestimated near this angle.

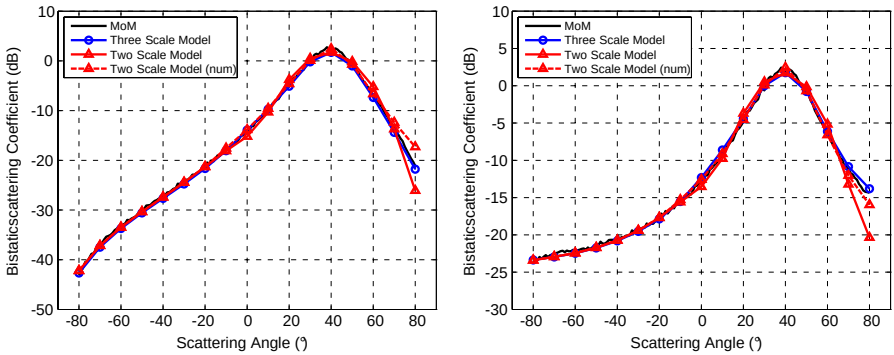

(a) Horizontal polarization (b) Vertical polarization

Figure 9. Bistatic scattering comparison. L band. Incidence angle: 40°. Wind speed: 3 m/s. (a) HH, and (b) VV.

4. CONCLUSIONS AND DISCUSSIONS

For bistatic scattering from 1-D ocean surfaces, we have carried out a systematic assessment of the performance of the popular TSM and its advanced version, namely, the T3SM, under different conditions of ocean surface wind speeds, polarizations, frequencies, and incidence angles. It is found that with the cut-off wavenumber set as $k/2\cos(\theta_i)$, the TSM model in general captures the bistatic scattering pattern, yet the accuracy of GO for the large scale wave brings considerable impact on the overall accuracy. The GO results fall off faster than its numerical counterpart (which is integrated numerically for the corresponding Kirchhoff integral), leading to observable discrepancy with MoM around the KA-SPM transition region of the scattered angles (Figs. 1 and 2). Further away from the GO peak, the first order SPM is found adequately accurate, hence the agreement between TSM and MoM is good. These features can be more readily observed when the incidence angle is in the range [10°, 50°]. If the evaluation of the

contribution of the large scale wave is instead using direct numerical integration for the Kirchhoff integral, impressive improvements are frequently observed, especially at low frequency (L and C bands) and low wind speed (3 m/s) (Fig. 6). But care should be taken when apply TSM with numerical integration, since there are cases where visible discrepancy with MoM are observed (Fig. 9).

On the other hand, T3SM is found in very good agreement with MoM across the considered ocean surface wind speeds, polarizations, frequencies, and incidence angles, hence represents a much advanced model over TSM.

Kasilingam and Shemdin [30] reported the existence of a maximum allowable wind speed for the composite surface model. For instance, at X-band and 25° incidence angle, the wind speeds cannot exceed 12 m/s for the composite surface model to be sufficiently accurate. And for a given incidence angle, the maximum allowable wind speed decreased with increasing frequencies. The current study does not suffer from the limitation on wind speed, hence the limits might be considered as an artifice of the choice of cut-off wavelength.

The radar cross-section of the ocean surface can be modulated by long surface waves and internal waves. The direct modulations include tilt modulation and the hydrodynamic modulation of the short waves, whereas an indirect modulation is due to the hydrodynamic modulation of the intermediate waves by the long waves. Tilting modulation leads to a change in the local incidence angle. The hydrodynamic modulation is prevalent mainly in the region where Bragg scattering predominates over specular scattering [30]. The current understanding of hydrodynamic modulation is still incomplete. For instance, when trying to include the indirect modulation (the "cascading modulation"), Plant found that the resultant modulations were much too large and frequently yielding negative spectral densities for the small waves [7]. For this reason we have chosen a minimalistic stand in this study by considering only the tilting modulation. However, the very good agreement of the composite surface models with MoM, in particular the T3SM model, across a wide range of sensor and sea state conditions, can be regarded as a pleasant surprise. The interpretation of the role of hydrodynamic modulations in the composite surface models, whose absence seems not bear much impact on the predictive power of these models, is a topic beyond the scope of this paper.

The insight furnished from 1-D study is certainly of value to the full 3-D surface scattering problem, sometimes with striking similarity between 1-D and 2-D results [31], yet caution should be taken when attempting to extrapolate the 1-D behaviors to 2-D cases.

APPENDIX A. ELFOUHAILY SPECTRUM

The original expression of the Elfouhaily spectrum was given in [25]. However [32] noticed that an additional term should be added. The spectrum employed in this study is as follows.

$$S_{EL}(k) = (B_L + B_H)/k^3 \tag{A1}$$

where $B_L = \alpha_p F_p c(k_p)/2c(k)$, and $B_H = \alpha_m F_m c(k_m)/2c(k)$. The two inputs are the wind speed at elevation of 10 m $U(10)$ and inverse wave age $\Omega \approx U(10)/c(k_p)$, which depend on phase speed $c(k)$ and spectral peak wavenumber k_p. Other parameters are defined as follows:

$$\alpha_p = 0.006\Omega^{1/2}, \quad k_p = g\Omega^2/U(10)^2, \quad g = 9.81,$$

$$c(k) = \left[g\left(1 + k^2/k_m^2\right)/k\right]^{1/2}, \quad k_m = 370\,\mathrm{m}^{-1}$$

$$F_p = \gamma^{\Gamma} \exp\left[-5(k_p/k)^2/4\right] \exp\left\{-\Omega\left[(k_p/k)^{1/2} - 1\right]/\sqrt{10}\right\}$$

$$\gamma = \begin{cases} 1.7 & 0.84 < \Omega \le 1 \\ 1.7 + 6\log(\Omega) & 1 < \Omega < 5 \end{cases},$$

$$\Gamma = \exp\left\{-\left[(k/k_p)^{1/2} - 1\right]^2 / 2\sigma^2\right\}, \quad \sigma = 0.08\left(1 + 4/\Omega^3\right),$$

$$\alpha_m = 0.01 \begin{cases} 1 + \ln[u/c(k_m)] & u \le c(k_m) \\ 1 + 3\ln[u/c(k_m)] & u > c(k_m) \end{cases},$$

$$C_{10} = (0.8 + 0.065U(10)) \times 10^{-3}, \quad u = C_{10}^{1/2} U(10),$$

$$F_m = \exp\left[-5(k_p/k)^2/4\right] \exp\left[-(1 - k/k_m)^2/4\right].$$

Wind speed $U(z)$ at the different elevation z in meters can be related by friction velocity u_*:

$$U(z) = \frac{u_*}{0.4} \ln\left(\frac{z}{z_0}\right) \tag{A2}$$

where $z_0 = \frac{0.0000684}{u_*} + 0.00428u_*^2 - 0.00443$.

ACKNOWLEDGMENT

The authors are grateful to the anonymous reviewers for their helpful reviews and suggestions. This work was supported by the National Natural Science Foundation of China under Grant No. 40976107.

REFERENCES

1. Silvestrin, P., M. Berger, Y. H. Kerr, and J. Font, "ESA's second earth explorer opportunity mission: The soil moisture and ocean salinity mission-SMOS," *IEEE Geosci. Remote Sens. Lett.*, Vol. 118, 11–14, 2001.
2. Gaiser, P. W., K. M. St. Germain, E. M. Twarog, G. A. Poe, W. Purdy, D. Richardson, W. Grossman, W. L. Jones, D. Spencer, G. Golba, et al., "The WindSat spaceborne polarimetric microwave radiometer: Sensor description and early orbit performance," *IEEE Trans. Geosci. Remote Sens.*, Vol. 42, No. 11, 2347–2361, 2004.
3. Wright, J. W., "A new model for sea clutter," *IEEE Trans. Antennas Propag.*, Vol. 16, No. 2, 217–223, 1968.
4. Lyzenga, D. R. and J. F. Vesecky, "Two-scale polarimetric emissivity model: Efficiency improvements and comparisons with data," *Progress In Electromagnetics Research*, Vol. 37, 205–219, 2002.
5. Soriano, G. and M. Saillard, "Modelization of the scattering of electromagnetic waves from the ocean surface," *Progress In Electromagnetics Research*, Vol. 37, 101–128, 2002.
6. Vaitilingom, L. and A. Khenchaf, "Radar cross sections of sea and ground clutter estimated by two scale model and small slope approximation in HF-VHF bands," *Progress In Electromagnetics Research B*, Vol. 29, 311–338, 2011.
7. Plant, W. J., "A stochastic, multiscale model of microwave backscatter from the ocean," *J. Geophys. Res.*, Vol. 107, No. C9, 3120, 2002.
8. Romeiser, R., A. Schmidt, and W. Alpers, "A three-scale composite surface model for the ocean wave-radar modulation transfer function," *J. Geophys. Res.*, Vol. 99, No. C5, 9785–9801, 1994.
9. Banks, C. J., C. P. Gommenginger, M. A. Srokosz, and H. M. Snaith, "Validating SMOS ocean surface salinity in the Atlantic with Argo and operational ocean model data," *IEEE Trans. Geosci. Remote Sens.*, Vol. 50, No. 5, 1688–1702, 2012.
10. Guimbard, S., J. Gourrion, M. Portabella, A. Turiel, C. Gabarró, and J. Font, "SMOS semi-empirical ocean forward model adjustment," *IEEE Trans. Geosci. Remote Sens.*, Vol. 50, No. 5, 1676–1687, 2012.
11. Wu, Z.-S., J.-P. Zhang, L.-X. Guo, and P. Zhou, "An improved two-scale model with volume scattering for the dynamic ocean

surface," *Progress In Electromagnetics Research*, Vol. 89, 39–56, 2009.

12. Sajjad, N., A. Khenchaf, A. Coatanhay, and A. Awada, "An improved two-scale model for the ocean surface bistatic scattering," *IEEE Trans. Geosci. Remote Sens. Symposium*, Vol. 1, I387–I390, 2008.
13. Voronovich, A. G., "Small-slope approximation for electromagnetic wave scattering at a rough interface of two dielectric half-spaces," *Waves Random Media*, Vol. 4, No. 3, 337–367, 1994.
14. Yang, G. and Y. Du, "A robust preconditioned GMRES method for electromagnetic scattering from dielectric rough surfaces," *IEEE Trans. Geosci. Remote Sens.*, Vol. 50, No. 9, 3396–3408, 2012.
15. Holliday, D., L. L. DeRaad, and G. J. St-Cyr, "Forward-backward: A new method for computing low-grazing angle scattering," *IEEE Trans. Antennas Propag.*, Vol. 44, No. 5, 722–729, 1996.
16. Chou, H. T. and J. T. Johnson, "A novel acceleration algorithm for the computation of scattering from rough surfaces with the forward-backward method," *Radio Sci.*, Vol. 33, 1277–1288, 1998.
17. Torrungrueng, D., J. T. Johnson, and H. T. Chou, "Some issues related to the novel spectral acceleration method for the fast computation of radiation/scattering from one-dimensional extremely large scale quasi-planar structures," *Radio Sci.*, Vol. 37, No. 2, 1019, 2002.
18. Li, S.-Q., C. H. Chan, L. Tsang, and L. Zhou, "Microwave emission of rough ocean surfaces with full spatial spectrum based on the multilevel expansion method," *IEEE Trans. Geosci. Remote Sens.*, Vol. 40, No. 3, 574–582, 2002.
19. Gill, E., W. Huang, and J. Walsh, "The effect of the bistatic scattering angle on the high-frequency radar cross sections of the ocean surface," *IEEE Geosci. Remote Sens. Lett.*, Vol. 5, No. 2, 143–146, 2008.
20. Ji, W.-J. and C.-M. Tong, "Bistatic scattering from two-dimensional dielectric ocean rough surface with a PEC object partially embedded by using the G-SMCG method," *Progress In Electromagnetics Research,* Vol. 105, 119–139, 2010.
21. Chen, H., M. Zhang, and H.-C. Yin, "Facet-based treatment on microwave bistatic scattering of three-dimensional sea surface with electrically large ship," *Progress In Electromagnetics Research*, Vol. 123, 385–405, 2012.
22. Tsang, L., J. A. Kong, and K. H. Ding, *Scattering of*

Electromagnetic Waves: Theories and Applications, John Wiley, 2000.

23. Johnson, J. T., R. T. Shin, J. A. Kong, L. Tsang, and K. Pak, "A numerical study of the composite surface model for ocean backscattering," *IEEE Trans. Geosci. Remote Sens.*, Vol. 36, No. 1, 72–83, 1998.
24. Johnson, J. T., "A numerical study of low-grazing-angle backscatter from ocean-like impedance surfaces with the canonical grid method," *IEEE Trans. Antennas Propag.*, Vol. 46, No. 1, 114–120, 1998.
25. Elfouhaily, T., B. Chapron, K. Katsaros, and D. Vandemark, "A unified directional spectrum for long and short wind-driven waves," *J. Geophys. Res.*, Vol. 102, No. C7, 781–769, 1997.
26. Thorsos, E. I., "Acoustic scattering from a 'Pierson–Moskowitz' sea surface," *J. Acoust. Soc. Am.*, Vol. 88, No. 1, 335–349, 1990.
27. Durden, S. and J. Vesecky, "A physical radar cross-section model for a wind-driven sea with swell," *IEEE J. Ocean. Eng.*, Vol. 10, No. 4, 445–451, 1985.
28. Bjerkaas, A. W. and F. W. Riedel, "Proposed model for the elevation spectrum of a wind-roughened sea surface," DTIC Document, Tech. Rep., 1979.
29. Ulaby, F. T., R. K. Moore, and A. K. Fung, *Microwave Remote Sensing: Active and Passive, Volume II: Radar Remote Sensing and Surface Scattering and Emission Theory*, Artech House, 1986.
30. Kasilingam, D. P. and O. H. Shemdin, "The validity of the composite surface model and its applications to the modulation of radar backscatter," *Int. J. Remote Sensing*, Vol. 13, No. 11, 2079–2104, 1992.
31. Li, Y. and J. C. West, "Low-grazing-angle scattering from 3-D breaking water wave crests," *IEEE Trans. Geosci. Remote Sens.*, Vol. 44, No. 8, 2093–2101, 2006.
32. McDaniel, S. T., "Small-slope predictions of microwave backscatter from the sea surface," *Waves Random Media*, Vol. 11, No. 3, 343–360, 2001.